ISSN (Print) 1226-1750
ISSN (Online) 2233-6656
Journal of Magnetics 22(2), 344-351 (2017) https://doi.org/10.4283/JMAG.2017.22.2.344

Wireless Magnetic Pump: Characteristics of Magnetic Impellers and Medical Application

Moon Kyou Song and Sung Hoon Kim*

Department of Electronics Convergence Engineering, Wonkwang University, 460 Iksandae-ro, Iksan, Jeonbuk 54538, Republic of Korea

(Received 28 May 2017, Received in final form 15 June 2017, Accepted 15 June 2017)

Wireless magnet pumps are used in medical applications and are particularly useful as artificial heart ventricular assist devices (VADs). To investigate wireless operation of magnetic pumps, we fabricated three types of magnetic impellers using bonded magnets by blending magnetic powders of SmFeN, NdFeB, and Sr-ferrite. We investigated the magnetic properties of the fabricated magnetic impellers, which are driven by the application of magnetic coupling with an external driving magnet or external coil system, without a driving motor, shaft, or mechanical bearings. The use of wireless magnetic pumps is therefore not complicated by critical issues of size, heat, and vibration, which are very important issues for blood pumps. The magnetic properties of the impellers, such as their rotational speed, driving torque and hydrodynamic performance, determine their wireless driving ranges. We conducted performance evaluations of the impeller's magnetic wireless manipulation, heat, and vibration. In addition, we carried out an animal test to confirm the suitability of the wireless magnetic pumps for use as biventricular assist devices (BiVADs).

Keywords : wireless magnetic pump, magnetic impeller, magnetic coupling, blood pump, magnetic powder

1. Introduction

Wireless magnetic technologies have been widely applied in biomedicine. Wireless magnetic actuators are used in minimally invasive treatments [1-5]. Magnetic torque and force controls based on electromagnetic (EM) or permanent magnet (PM) controls are notable means of manipulation of wireless magnetic actuators [6-9]. Many applications of wireless magnetic actuators in the use of robotics in medicine have been reported. Notable biomedical applications of wireless magnetic actuators have been in pump systems. Depending on their scale, wireless magnetic pumps can be used in various pump applications, such as microfluid manipulation and blood pumps [10-12]. Since the 1960's, artificial heart system technology has developed steadily. First-generation artificial heart pumps were pulsatile pumps [13-15]. Second-generation artificial heart pumps were centrifugal flow-type pumps [16-18]. Recently, third-generation artificial heart pumps have been developed using magnetically levitated rotors [19-21]. However, all artificial heart ventricular assist devices (VADs) developed to date have used either power cables that pass through skin or wireless power transmission with implantable batteries. These methods of powering artificial hearts can cause bacterial infections related to power cables in the skin or replacement of implantable batteries.

In a previous study, we introduced the concept of wireless magnetic blood pumps and techniques for using them to overcome the issues associated with other methods of powering artificial hearts. These techniques include wireless magnetic operation, use of magnetic impellers, and tests of left ventricular assist devices [22]. In addition, a wireless pump can be configured to prevent problems of heat generation and vibration, which are important concerns associated with the use of implantable pump systems.

In this study, we investigated the magnetic properties of magnetic impellers developed using bonded magnet technology and the effects of those magnetic properties on wireless magnetic operation of such impellers and their pumping ability. Wireless magnetic pumps produce less heat and vibration than other types of pumps because they do not have electrical motors, shafts, and mechanical bearings. The developed pump adopts the concept of hydro-

*Corresponding author: Tel: +82-63-850-6739
Fax: +82-63-850-6739, e-mail: kshoon@wku.ac.kr

dynamic bearings instead of a mechanical bearings. Heat and vibration are very important factors in the performance of artificial heart systems. We analyzed the heat and vibration produced by wireless magnetic pumps over a period of 10 h for a range of driving distances and a range of rotational speeds of the magnetic impellers. We also conducted an animal test in which we installed a pump for a biventricular assist device (BiVAD) and evaluated its pumping ability during stable circulation over a period of 6 h. Finally, we performed hematocrit testing to check the separation ratio of blood cells per hour over a period of 6 h.

2. Magnetic Properties of Magnetic Impeller and Wireless Operation

2.1. Magnetic properties of the fabricated magnetic impeller

To create a wireless pump, we developed a magnetic impeller using bonded magnet technology and an external driving magnet. The wireless magnetic pump is driven by an electromagnetic (EM) control or a permanent magnet (PM) control. An EM control uses a pair of two coils to generate a uniform rotating magnetic field. The magnetic impeller is synchronized by the rotating magnetic field. In this case, the driving torque becomes a magnetic torque. A PM control uses radial and axial magnetic couplings between an external driving magnet and the magnetic impeller based on a coupling force.

Although EM control has greater controllability than PM control, it has the critical problem of heat generation from the driving coils. Therefore, the magnetic properties of the magnetic impeller are very important. Although a permanent magnet cannot control the magnetic field strength, it can be easily replaced. Hence, PM control permits relatively weaker magnetic properties for the magnetic impeller than EM control.

In general, sintered magnets cannot be used to form complex shapes. Therefore, we fabricated and investigated the magnetic properties of three types of magnetic impellers: one with 50 wt% SmFeN with a polyphenylene sulfide (PPS) resin, one with 50 wt% Sr-ferrite with a polyamide type A (PA12) resin, and one hybrid type with 50 wt% Sr-ferrite and NdFeB with a PA12 resin. The magnetic impellers were fabricated by injection molding.

We analyzed the magnetic properties of fabricated rectangular samples with volumes of 0.018 cm^3 using vibration sample measurement (VSM), as shown in Fig. 1. The VSM analysis allowed us to compare the magnetic properties of the samples, such as their magnetic moments (***m***) and coercive forces (H_c). The SmFeN sample, which

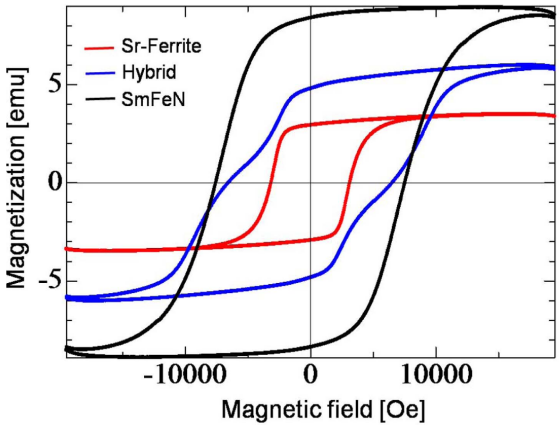

Fig. 1. (Color online) Magnetic properties of three magnetic samples: Sr-ferrite, hybrid-type (NdFeB + Sr-ferrite), and SmFeN. The sample volumes were 0.0183 cm^3.

had a magnetic moment of 8.385×10^{-3} Am^2 (8.385 emu) and a coercive force (H_c) is 0.6×10^6 A/m, had the strongest magnetic properties. The hybrid-type sample had a magnetic moment of 4.812×10^{-3} Am^2 (4.812 emu) and a coercive force of 0.521×10^6 A/m. The Sr-ferrite sample had a magnetic moment of 2.931×10^{-3} (2.931 emu) and a coercive force of 0.25×10^6 A/m. Injection-molded magnetic impellers can be very simple in shape or very complex. Multi-stage backward curvature blades, as shown in Fig. 2, were formed inside the magnetic impellers we fabricated.

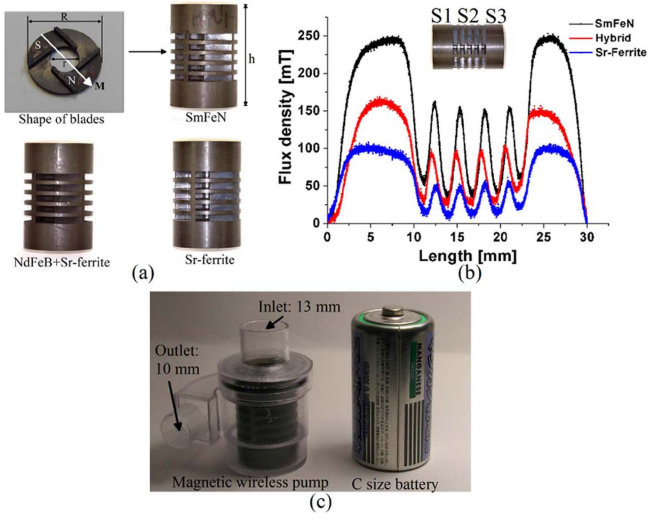

Fig. 2. (Color online) (a) Magnetic impellers fabricated using an injection molding process: R = 19.7 mm, r = 7.5 mm, and h = 30 mm, blade thickness = 2 mm. (b) Surface magnetic flux density in the radial direction of the magnetic impellers. S1, S2, and S3 are sections of the magnetic impeller. (c) Fully assembled magnetic wireless pump and a C battery shown for size comparison.

Table 1. Properties of magnetic impellers.

	m [Am^2]	Hc [A/m]	Ratio [wt%]	Resin
Sr-ferrite	0.816	0.25×10^6	50	PA12
Hybrid	1.341	0.521×10^6	50	PA12
SmFeN	2.336	0.6×10^6	50	PPS

The magnetic impellers that we fabricated had four blade sections. A single stage consisted of four blades at 30° angles. The blades were 2 mm in thickness. The total lengths and diameters of the magnetic impellers were 30 mm and 20 mm, respectively. The magnetization of the impeller was in the radial direction to achieve synchronous radial magnetic coupling with an external driving magnet. Table 1 lists some of the properties of the three of magnetic impellers. The magnetic moment of each impeller is proportional to the volume. The total volume of each impeller is 5.1 cm^3. The SmFeN impeller had a magnetic moment of 2.336 Am^2. The hybrid-type and Sr-ferrite impellers had magnetic moments of 1.341 Am^2 and 0.816 Am^2, respectively. We investigated the distribution of the magnetic flux density on the surface of each magnetic impeller using a Gauss meter, as shown in Fig. 2(b). The distributed flux densities were not uniform because of the shapes of the magnetic impellers. Sections Sl and S3 were a cylindrical in shape, and section S2 consisted of multi-stage blade parts. Because of the shapes of the impellers, the distributions of the flux density were different. The magnetic flux density of the SmFeN-based impeller was approximately three times higher than that of the Sr-Ferrite-based impeller.

The magnetic wireless pump developed consisted of a magnetic impeller and a pump housing, with no mechanical bearings, shafts, or assembled electrical motor, as shown in Fig. 2(c), in which the size of the pump is illustrated by comparison with a C-type battery. The Inlet and outlet diameters were 13 mm and 10 mm, respectively. The total weight of the pump was 53 g.

2.2. Properties of wireless magnetic operation using a magnetic coupling

The magnetic impellers were driven by magnetic radial coupling using an external magnet, as shown in Fig. 3(a). The external driver consisted of a direct current (DC) motor and the driving magnet. The different impellers created different coupling forces because of their different magnetic properties. Figure 3(b) shows the magnetic coupling forces between the magnetic impellers and the external driving magnet as a function of the air gap. We measured the coupling forces for air gap up to 4 cm. The

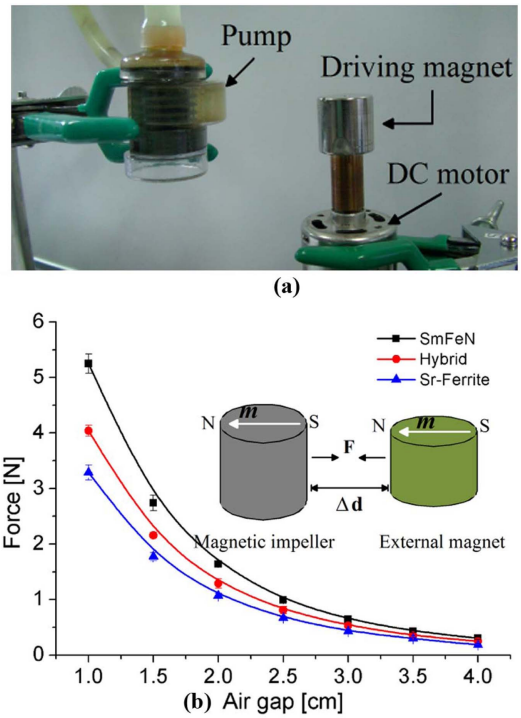

Fig. 3. (Color online) (a) A wireless control of the pump using a synchronous radial coupling. (b) Observation of magnetic coupling forces between the magnetic impeller and the external magnet, where ***m*** is the magnetic moment and white arrows are a direction of magnetic moment. **F** is the magnetic coupling force. **Δd** is an air-gap between the impeller and the external magnet.

external driving magnet was a cylindrical NdFeB permanent magnet with radial magnetization, 20 mm in diameter and 20 mm in height. The surface magnetic flux density and adsorption power of the external driving magnet were 543 mT and 15.4 kg, respectively.

The magnetic coupling between the impeller and the driving magnet depends on the magnetic properties and the size of the impeller with the driving magnet. In addition, because of portability the driving system, the maximum size of the driving magnet is limited to the size of the impeller.

Typically, the magnetic coupling force varies nonlinearly with respect to distance. The three types of impellers exhibited significantly different coupling forces between their respective maximums and minimums because of their different magnetic properties (see Table 1). The SmFeN-based impeller, which had the strongest magnetic properties, generated maximum and minimum forces of 5.248 N and 0.304 N at air gaps of 1 cm and 4 cm, respectively. Under equivalent conditions, the hybrid-type impeller generated maximum and minimum forces of 2.157 N and 0.25 N, respectively, and the Sr-ferrite-based

impeller generated maximum and minimum forces of 1.774 N and 0.185 N. The coupling forces depended greatly on the magnetic properties of the impeller at closer distances. Although a small air gap produced a high coupling force, it also resulted in several problems, such as high power consumption by the external driver and limited rotation speed because of increased starting torque.

When the coupling force exceeded approximately 2.5 N, the pump's behavior reflected these problems. For an air gap of 1.5 cm, the hybrid-type and Sr-ferrite-based impellers produced stable operation, whereas the SmFeN-based impeller produced a stable operation at an air gap of 2 cm. Although an air gap difference of 0.5 cm is small, the difference in the coupling force is large because the coupling force is related nonlinearly to the distance. In the pump system developed in this study, a coupling force of 2.5 N was a threshold for stable operation.

As mentioned above, the rotation speeds of the impellers were limited by the coupling forces produced as a function of the magnetic properties of the impellers

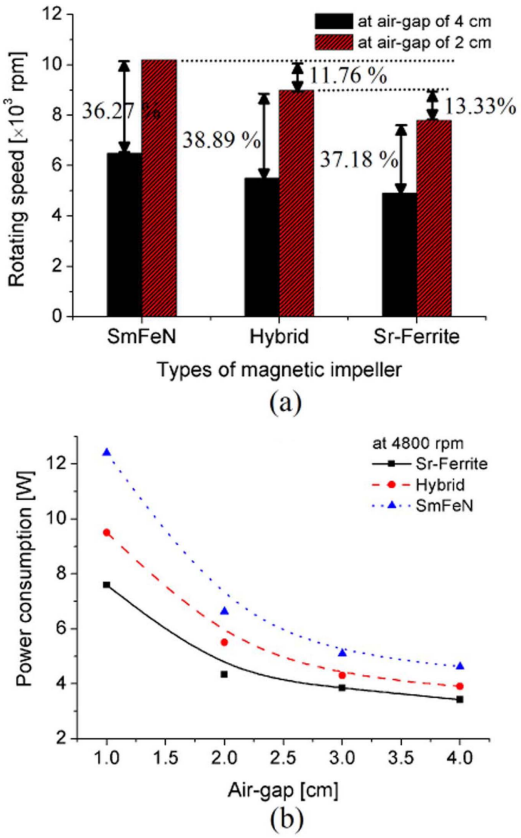

Fig. 4. (Color online) (a) Observations of rotation speed for the three types of magnetic impellers at coupling distances of 2 and 4 cm. (b) Power consumption for the three types of magnetic impellers as a function of the coupling distance for a fixed rotation speed of 4800 rpm.

because the coupling force is a physical load on a DC motor (the external driver). We investigated the driving ranges of the pump with respect to the types of impeller and the magnetic coupling distance, as shown in Fig. 4(a). We were able to confirm that the driving features of the pump depend on both the magnetic properties of the impeller and the driving distance. The driving distance between the impeller and the external driver is a dominant factor in determining the rotation speed of the pump. We first considered a driving range base on the type of material used for a fixed air gap.

In this case, the SmFeN-based impeller produced a maximum speed of 10,200 rpm at an air gap of 2 cm (corresponding to a coupling force of 1.64 N). The hybrid-type and Sr-ferrite-based impellers produced maximum speeds of 9000 rpm and 7800 rpm, respectively, at a coupling distance of 2 cm. These speeds correspond to driving speed decreases of 11.76 % and 13.33 %, respectively. We then changed the coupling distance from 2 cm to 4 cm and determined the maximum speed produced by each impeller. The maximum speed of the SmFeN-based impeller decreased from 10,200 rpm to 6,500 rpm, a decrease of approximately 36.27 %, and the hybrid-type and Sr-ferrite-based impellers decreased by 38.89 % and 37.18 %, respectively, to 5,500 and 4,900 rpm, respectively.

Figure 4(b) illustrates the power consumption of the external driver (the DC motor) as a function of the coupling distance for a fixed driving speed of 4800 rpm. The power consumption of the external driver was 2.98 W at no load. At a coupling distance of 1 cm, the SmFeN-based impeller, hybrid-type, and Sr-ferrite-based impellers consumed 12.4 W, 9.5 W and 7.56 W, respectively. At a coupling distance of 2 cm, the SmFeN-based, hybrid-type, and Sr-ferrite-based impellers consumed 6.22 W, 5 W, and 4.3 W, respectively–a decrease of 44 % on average. At a coupling distance of 4 cm, the SmFeN-based, hybrid-type, and Sr-ferrite-based impellers consumed 4.62 W, 3.9 W, and 3.42 W, respectively.

In these analyses, the SmFeN-based impeller was found to have the widest driving ranges (coupling distance and rotation speed) of the three impeller types, and it consumed the most power at any given coupling distance. Although the SmFeN-based impeller has several advantages, the price of magnetic SmFeN powder is approximately ten times higher than that of magnetic Sr-ferrite powder. The price of hybrid-type material is between that of SmFeN and that of Sr-ferrite. If we take both the desired performance of the impeller and the cost into consideration, a hybrid-type or Sr-ferrite-based impellers becomes a leading candidate for use in a wireless pump system.

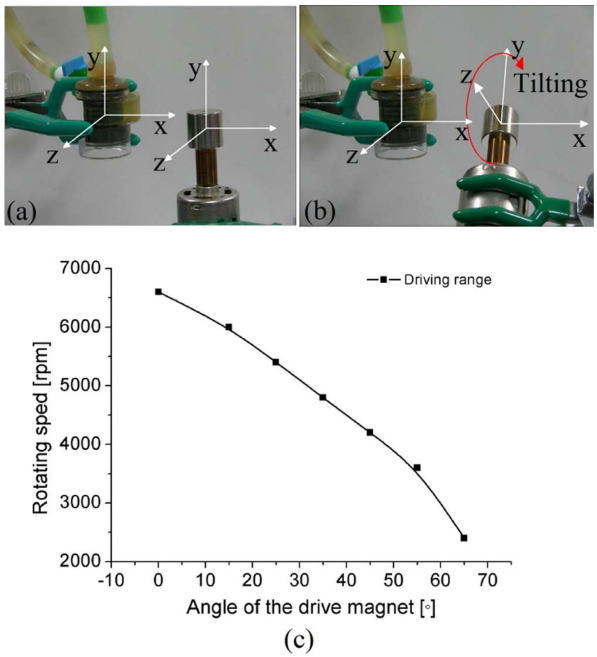

Fig. 5. (Color online) Analysis of driving range with respect to changes in the tilt angle: (a) Initial radial coupling at approximately 4 cm. (b) The tilted driving magnet with a radial coupling. (c) Relationship between the rotation speed of the impeller and the tilt angle.

We investigated the operating features of each of the impellers when the rotational plane of the impeller and that of the external magnet were (i.e., a tilt angle of 0°) in a three-dimensional coordinate system, as shown in Fig. 5(a). We observed the effect on the driving range of changes (in intervals of 15°) in the tilt angle about the x-axis (roll motion) for a fixed coupling distance of approximately 4 cm, as shown in Fig. 5(b). As the tilt angle increased from 0 to 65° in interval of 15°, the rotation speed of the impeller decreased to 2400 rpm in intervals of approximately 600 rpm, as shown in Fig. 5(c). When the angle exceeded 65°, the driving magnet stopped rotating the impeller because the rotation axis of the driving magnet approached z-axis; that is, the magnetic torque direction changed from that of the y-axis to that of z-axis. The driving magnet exhibited similar behavior for yaw motion and pitch motion. The hybrid-type and Sr-ferrite-based impellers produced similar results for tilt angles up to 65° at a shorter coupling distance of less than 2 cm.

3. Analysis of Vibration and Heat Generation During Pump Operation

Typical pump systems, which consist of an electrical

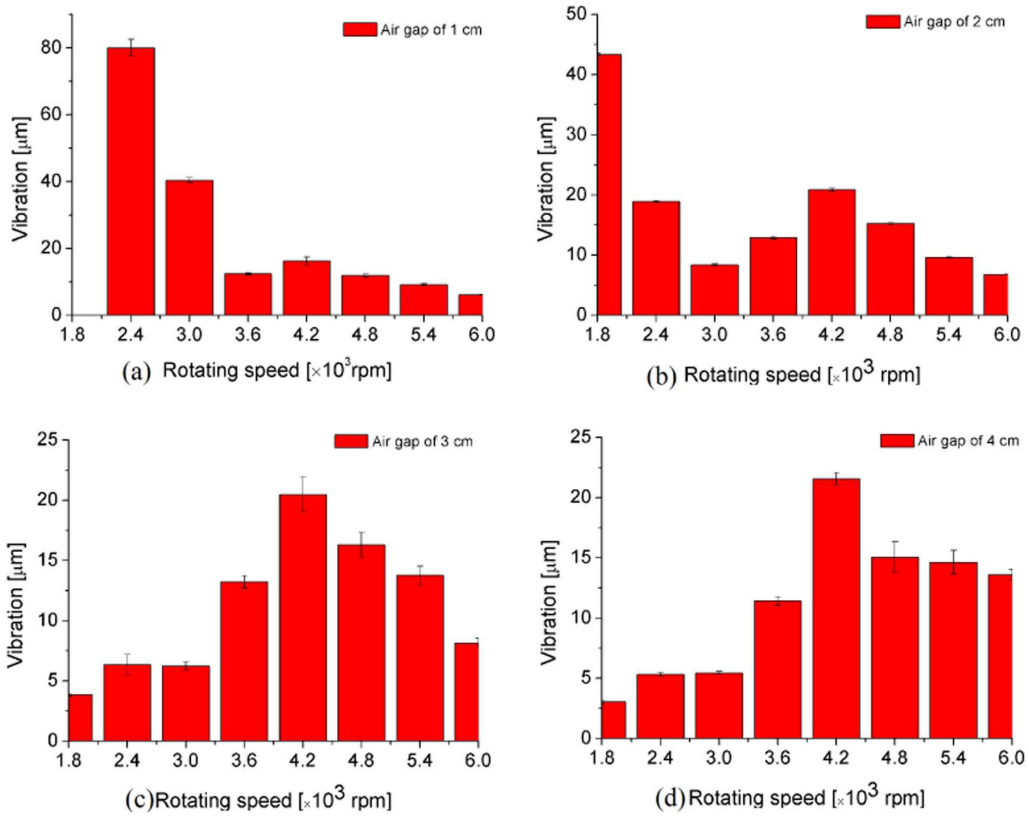

Fig. 6. (Color online) Vibration characteristics of the proposed pump using a SmFeN-based impeller for coupling distances from 1 to 4 cm and a rotation speeds up to 6000 rpm.

motor, a shaft, and mechanical bearings, generate heat and vibration because of the pump configuration. These are critical problems for an implantable blood pump system. A liquid-cooled artificial heart pump system has been developed to attempt to address these problems [23]. The configuration of this pump does not include an electrical motor, a shaft, and mechanical bearings. We investigated the heat generation and vibration characteristics of this pump experimentally. First, we measured the effect on vibration of coupling distances from 1 cm to 4 cm and rotation speeds from 1800 rpm to 6000 rpm, using an OH-580A vibration meter (TESTO, Inc., Sparta, New Jersey, USA).

The measured vibrations were found to depend on the coupling distance and the rotation speed. Figure 6(a) shows the effect of rotation speed on vibration for a coupling distance of 1 cm. Because of the high coupling force at this short distance, the pump was unable to operate at a rotation speed of 1800 rpm. The largest vibrations, averaging 80.03 μm, occurred at a rotation speed of 2400 rpm because of the high coupling force.

The vibration magnitudes decreased dramatically with increasing rotation speed: at 3600 rpm, the average vibration magnitude was 12.4 μm. The absolute values of the vibrations were smaller at a coupling distance of 2 cm, but the trend was the same: lower rotation speeds generated large vibration because of the large coupling force.

In contrast, when the coupling distance was greater (i.e., 3 or 4 cm), low rotation speeds produced relatively small vibrations, especially at 1800 rpm and 2400 rpm, as shown in Fig. 6(c) and (d).

Under these conditions, the pump generated vibrations of less than 5 μm. Furthermore, the vibrations increased with increasing rotation speed, peaking at a rotation speed of 4200 rpm. The vibrations then decreased with increasing rotation speed beyond 4200 rpm. The maximum vibration averaged approximately 20 μm at 4200 rpm. This trend was observed for all of the coupling distances considered. In other words, the pump has a resonance point for vibration at a rotation speed of 4200 rpm (70 Hz), regardless of the coupling distance and force. Apart from those at 4200 rpm, the vibrations generated by the pump were less than 15 μm. The hybrid-type and the Sr-ferrite-based impellers exhibited almost same vibration trends as the SmFeN-based impeller in the driving range of 3000 to 6000 rpm. The differences in the vibrations for the difference types of impeller were less than approximately 8 %. However, when the coupling distance was 1 cm, the first two impellers exhibited a decrease in the average maximum vibration of approximately 20 %, compared to the SmFeN-based impeller, at a rotation speed of 2400 rpm because of the relatively low coupling force between the impellers and the driving magnet.

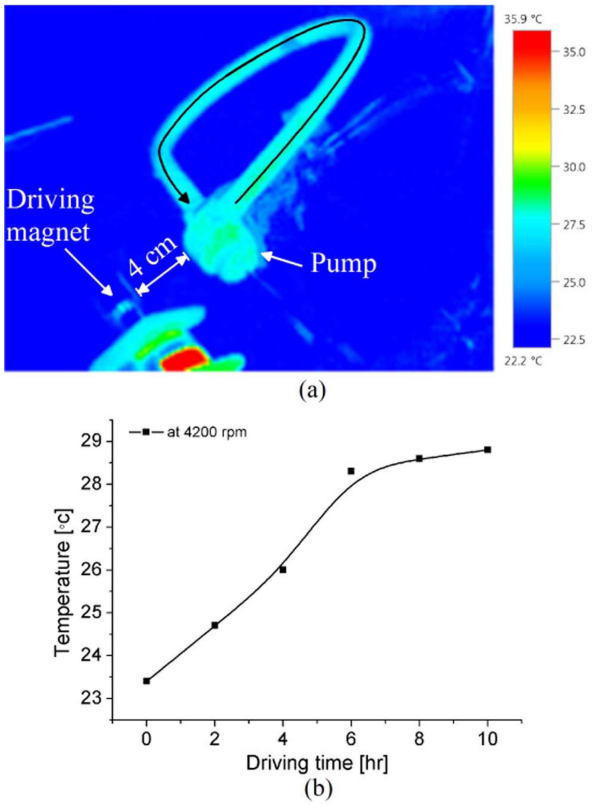

Fig. 7. (Color online) Heat distribution during water circulation: (a) Measurement of heat distribution using thermal imaging camera after circulation for 10 h at 4200 rpm; the type of liquid is water. (b) Change in heat generation over 10 h at 4200 rpm.

For this pump, rotation speeds of 3000 to 6000 rpm correspond to pumping volumes of approximately 4.2 to 10 L/min, which is suitable hemodynamic performance for an artificial heart pump system. Thus, low pump vibration is very important at a rotation speed of 6000 rpm.

We next observed the heat generation of the pump over a period of 10 h using a thermal imaging camera (Testo-875, Testo, Inc., Sparta, New Jersey, USA). As mentioned previously, the pump does not have mechanical bearings and an internal shaft. Because of the concept of hydrodynamic bearing, we expected low heat generation. Figure 7 showed the results of the observation of heat generation during operation of the pump. For the experiment, we installed a closed-loop circulation system using water as the liquid. The coupling distance between the pump and the external magnet was fixed a 4 cm. The rotation speed of the pump was fixed at 4200 rpm because that speed had been found to correspond to maximum vibration, as

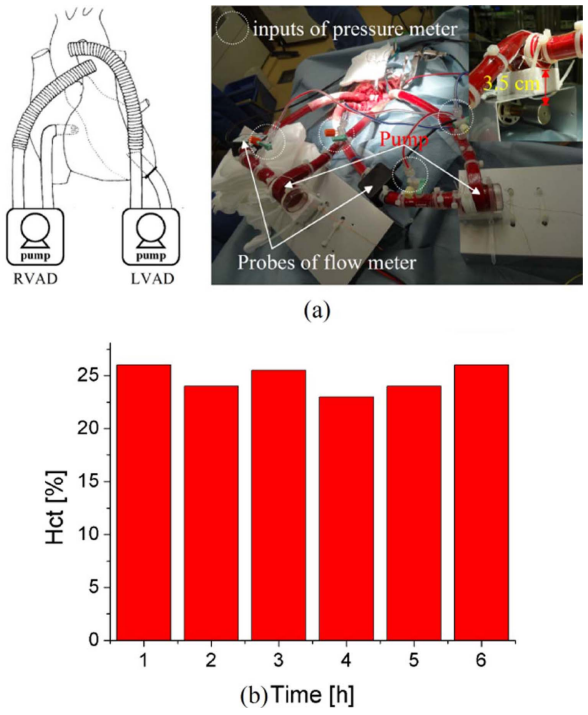

Fig. 8. (Color online) Animal test: (a) Application of BiVAD and system configuration. (b) Results of hematocrit tests to determine separation ratio of blood cells.

shown in Fig. 6. Figure 7(a) shows a thermal image of the pump with the external driver, captured by the thermal imaging camera after 10 h of operation. The peak temperature measured was 28.8°C at 4200 rpm. When we started the experiment, the water temperature was 23.4°C. We measured the pump temperature at intervals of 2 h for a total of 10 h. The pump's temperature increased linearly during the first 6 h from 23.4 to 28.3°C. The temperatures at 8 and 10 h were 28.6°C and 28.8°C, respectively. When the driving time exceeded 8 h, the rate of temperature increase dropped off dramatically and the heat generation appeared to reach a steady state. Thus, the proposed pump was able to avoid the problem of excessive heat generation. Heat generation is very important in a blood pump because high temperatures can cause blood clots.

4. Application of BiVAD

The proposed pump system was found to exhibit minimal problems with vibration and heat generation. These two problems are particularly important blood pump. We employed the pump in a biventricular assist device (BiVAD) used to conduct an animal test. This pump is very small, being a centrifugal flow pump, in comparison to a typical blood pump. Because a BiVAD system requires two pumps to assist both the left and right sides of the heart, pump size is very important. For this reason, and to minimize vibration and heat generation, we used the pump in a BiVAD device. Typically, a left ventricular assist device (LVAD) requires a lower-than-average flow rate of 10 L/min for adults and a flow rate of less than 2 L/min for young children. A right ventricular assist device (RVAD) requires a flow rate of less than 3 L/min. The pump investigated in this study produced a maximum flow rate of 10 L/min at 6000 rpm. Figure 8(a) shows the pump installed in a BiVAD for testing conducted using a goat weighting 38 kg. The coupling distance between the pump and the external magnet was fixed at 3.5 cm. For the RVAD system, we limited the rotation speed to the range of 1000 to 3000 rpm, and for balanced circulation, we limited the rotation speed of the LVAD system to the range of 4000 to 6000 rpm. Under the conditions of the test, the RVAD system generated a maximum flow rate of approximately 3.2 L/min, and the LVAD system generated a maximum flow rate of approximately 5.5 L/min. These pumping abilities satisfied the requirements for a BiVAD. We conducted hematocrit testing to observe the blood damage caused: the separation ratio of the blood cells average less than 25 %, as shown in Fig. 8(b).

5. Conclusion

In this study, we conducted two sets of analyses of the performance of wireless magnetic impellers for use in blood pumps: an analysis of the magnetic properties of three impellers and an analysis of their mechanical properties–specifically, vibration and heat generation in a pump equipped with a wireless magnetic impeller. We first compared the magnetic properties of three types of magnetic impellers produced by injection molding. We found that the magnetic properties of the impellers determined the driving factors, namely, the coupling distance, the coupling force, the power consumption of the external driver, and the rotation speed of the impeller. Impellers with stronger magnetic properties produce higher coupling forces, longer coupling distances, and higher rotation speeds, but they result in higher power consumption by the external driver and limit the ability of the impeller to operate at low rotation speeds at short coupling distances. Thus, strong magnetic impellers are suitable for high-speed pump control and greater coupling distances. Impellers with weaker magnetic properties have narrower driving ranges but are more suitable for low-speed pump control because of the relatively lower coupling forces that they produce. If the pump is implanted in the body, the pump can be fixed in the body because the pump is

placed in close contact with inside of the body and the distance between the pump and the driving magnet controls the coupling force. In addition, when the impeller rotates, the pulling force between the magnets is decreased. Through the animal test, we verified the problem in the previous study.

We next analyzed the vibration and heat generation of the proposed pump system. As mentioned above, the major advantages of the configuration of this pump system are low vibration and heat generation. The pump was found to have sufficient pumping ability at rotation speeds from 3000 to 6000 rpm for use in a blood pump. Under the test conditions, the pump produced maximum vibrations averaging 20 μm at a rotation speed of 4200 rpm. However, at other speeds, very small vibrations, averaging less than 15 μ, were generated. In general, vibration can cause heat generation. However, the vibrations generated by the pump were sufficiently small that they did not cause heat generation. When we observed heat generation over a period of 10 h, temperature less than 30°C were maintained. Thus, the amount of heat generated by the pump is sufficiently small that it does not affect blood damage. In addition, because body temperature is constant around 36°C and cooling is done by blood flow, we cannot observe maximum heat generation at the constant body temperature. Thus, we performed the experiment at room temperature. This was verified by hematocrit testing during the animal test, in which the pump was used in a BiVAD application. The pump was found to produce sufficient blood flow and blood pressure for balanced circulation of the left and right sides of the heart. The proposed pump system is quite small and functions as a simple centrifugal-type pump because of the bonded magnet techniques used in its production and its wireless magnetic means of operation. The utilized magnetic materials for the impeller are not biocompatible. Therefore, the fabricated impeller should be coated with a biocompatible materials on the surface, such as covalently bonded heparin coating.

Acknowledgments

This research was supported by Wonkwang University in 2015.

References

[1] B. J. Nelson, K. Kaliakatsos, and J. J. Abbott, Annu. Rev. Biomed. Eng. **12**, 55 (2010).
[2] K. B. Yesin, K. Vollmers, and B. J. Nelson, JIJRR. **25**, 527 (2006).
[3] S. H. Kim and K. Ishiyama, IEEE/ASME Trans. Mechatron. **19**, 1651 (2014).
[4] T. Fukushi, S. H. Kim, S. Hashi, and K. Ishiyama, Smart Mater. Struct. **23**, 607001 (2014).
[5] S. G. Kim, F. Qiu, S. H. Kim, A. Ghanbari, L. Zhang, and B. J. Nelson, Adv. Mater. **25**, 5863 (2013).
[6] S. Jeon, G. Jang, H. Choi, and S. Park, IEEE Trans. Magn. **46**, 1943 (2010).
[7] S. H. Kim, K. S. Shin, S. Hashi, and K. Ishiyama, IEEE Trans. Magn. **49**, 3488 (2013).
[8] S. H. Kim, J. W. Shin, and K. Ishiyama, IEEE Trans. Magn. **50**, 4003404 (2014).
[9] A. Mahoney and J. J Abbott, IEEE Trans. Robot. **30**, 411 (2014).
[10] M. Du, X. Ye, K. Wu, and Z. Zhou, Sensors **9**, 2611 (2009).
[11] A. Yamazaki, M. Sendoh, K. Ishiyama, K. I. Arai, and T. Hayase, IEEE Trans. Magn. **39**, 3289 (2003).
[12] L. Yobas, K. C. Tang, S. E. Yong, and E. K-Z. Ong, Lab. on a Chip. **8**, 660 (2008).
[13] J. Waaben, K. Andersen, and B. Husum, J. Thorac. Cardiovasc. Surg. **19**, 149 (1985).
[14] F. Inzoli, E. Di Martino, G. Dubini, A. Redaelli, and R. Fumero, Int. J. Artif. Organs **19**, 359 (1996).
[15] W. Y. Moores, E. R. Kahn, M. M. Kirsh, O. Gago, E. A. Carrjr, G. D. Abrams, J. Dufek, and H. Sloan, Ann. Thorac. Surg. **12**, 262 (1971).
[16] Y. Wakisaka, T. Taenake, K. Chikanari, Y. Okuzono, S. Endo, and H. Takano, ASAIO J. **43**, 608 (1997).
[17] T. Yamame, J. Artif. Organs **5**, 149 (2002).
[18] D. J. Burke, E. Burke, F. Parsie, V. Poirier, K. Butler, D. Thomas, L. Taylor, and T. Maher, Artif. Organs **25**, 380 (2001).
[19] A. Hilton and G. Tansley, Artif. Organs **32**, 772 (2008).
[20] W. Hijikata, T. Shinshi, J. Asama, L. Li, H. Hoshi, S. Takatani, and A. Shimokohbe, Artif. Organs **32**, 1 (2008).
[21] W. Hijikata, H. Sobajima, T. Shinshi, Y. Nagamine, S. Wada, S. Takatani, and A. Shimokohbe, Artif. Organs **34**, 669 (2010).
[22] S. H. Kim, K. Ishiyama, S. Hashi, Y. Shiraishi, Y. Hayatsu, M. Akiyama, Y. Saiki, T. Yambe, Artif. Organs **37**, 920 (2013).
[23] J. W. Mulholland, J. C. Shelton, and X. Y. Luo, J. Fluids Struct. **20**, 129 (2005).